Journal of Power Sources 188 (2009) 453–457

Contents lists available at ScienceDirect

Journal of Power Sources

journal homepage: www.elsevier.com/locate/jpowsour

Short communication

$(La_{0.74}Bi_{0.10}Sr_{0.16})MnO_{3-\delta}$–$Ce_{0.8}Gd_{0.2}O_{2-\delta}$ cathodes fabricated by ion-impregnating method for intermediate-temperature solid oxide fuel cells

Junliang Li, Shaorong Wang*, Zhenrong Wang, Renzhu Liu, Xiaofeng Ye, Xiufu Sun, Tinglian Wen, Zhaoyin Wen

Shanghai Institute of Ceramics, Chinese Academy of Sciences, 1295 Dingxi Road, Shanghai 200050, PR China

ARTICLE INFO

Article history:
Received 6 November 2008
Received in revised form 8 December 2008
Accepted 8 December 2008
Available online 13 December 2008

Keywords:
Intermediate-temperature solid oxide fuel cells
Composite cathode
Impedance spectroscopy
Ion-impregnation

ABSTRACT

Porous composite cathodes were fabricated by impregnating $(La_{0.74}Bi_{0.10}Sr_{0.16})MnO_{3-\delta}$ (LBSM) electronic conducting structure with the ionic conducting $Ce_{0.8}Gd_{0.2}O_{2-\delta}$ (GDC) phase. The ion impregnation of the GDC phase significantly enhanced the electrocatalytic activity of the LBSM electrodes for the O_2 reduction reactions, and the ion-impregnated LBSM–GDC composite cathodes showed excellent performance. At 700 °C, the value of the cathode polarization resistance (Rc) was only 0.097 Ω cm^2 for an ion-impregnated LBSM–GDC cathode, and the performance was gradually improved by increasing the loading of the impregnated GDC. For the performance testing of single cells, the maximum power density was 1036 mW cm^{-2} at 700 °C for a cell with the LBSM–GDC cathode. The results demonstrated the unique combination of the LBSM electronic conducting structure with high ionic conducting GDC phase was a valid method to improve the electrode performance, and the ion-impregnated LBSM–GDC was a promising composite cathode material for the intermediate-temperature solid oxide fuel cells.

1. Introduction

The solid oxide fuel cell (SOFC) has emerged as one of the most important power generation device because of its high-energy conversion efficiency, low noise and low pollution [1–3]. For solid oxide fuel cells, their performance is closely linked with their electrode materials. $La_{1-x}Sr_xMnO_{3-\delta}$ (LSM) perovskite is one of the cathode materials for solid oxide fuel cells. However, due to its low ionic conductivity and high activation energy for oxygen disassociation, pure LSM is limited in the application of cathodes for SOFC operating at intermediate-temperatures (600-800 °C). $La_{1-x}Sr_xCo_{1-y}Fe_yO_{3-\delta}$ (LSCF) perovskite has been shown to display two to four orders of magnitude higher oxygen permeation fluxes than the LSM cathode at identical operating temperatures [4]. However, LSCF has an incompatible thermal expansion coefficient (TEC) and high reactivity with yttrium-stabilized zirconia (YSZ) [5], which is the standard electrolyte material currently in use. So, it is necessary to improve the performance of the LSM cathode. It is reported that the composite cathodes can availably improve its electrochemical performance [6]. It was shown that by adding 50 wt.% YSZ to the LSM cathode, the polarization resistance could be reduced to 25% of its original value. Subsequent studies showed improvements using a variety of cathode arrangements and fabrication methods [7–11]. Gadolinia-doped ceria (GDC) is a better material for this application because its ionic conductivity is higher than that of YSZ [12–14]. The composite structure has been shown to be very promising in improving electrode performance. For instance, the interfacial polarization resistances (area-specific resistance) were 2.49 and 0.75 Ω cm^2 for a LSM–YSZ cathode and a LSM–GDC cathode, respectively [10,15].

Now, a more effective ion-impregnating method has been proposed to fabricate the composite cathodes [16–19]. It is an effective way to deposit electrocatalytic oxide phase into the porous LSM structure without diminishing the advantages of stability and compatibility of LSM materials with YSZ electrolyte.

In our previous study, we have developed the LBSM cathode and shown its better performance than the LSM cathode [20]. And in this study, LBSM–GDC composite cathodes for intermediate-temperature SOFCs based on the SSZ electrolyte were fabricated with a two-step fabricating process including screen-printing and ion-impregnating, and the electrochemical behavior at the cathode/electrolyte was investigated by AC-impedance analyses. Besides, the performance of anode-supported single cells using LBSM–GDC as cathode material was evaluated.

2. Experimental

The LBSM powder was synthesized by autoignition of citrate–nitrate gel, as described before [20]. The LBSM and SSZ

* Corresponding author. Tel.: +86 21 52411520; fax: +86 21 52413903.
E-mail address: srwang@mail.sic.ac.cn (S. Wang).

0378-7753/$ – see front matter © 2008 Elsevier B.V. All rights reserved.
doi:10.1016/j.jpowsour.2008.12.027

$((ZrO_2)_{0.89}(Sc_2O_3)_{0.1}(CeO_2)_{0.01}$, Tosoh, Japan) powders were pressed uniaxially into cylinders 5 mm in diameter and 20 mm in length. The LBSM and SSZ cylinders were sintered in air for 10 h at 1200 and 1500 °C, respectively, and then were used to measure the thermal expansion coefficient (TEC). The density was greater than 93% of the theoretical value for the two materials.

To prepare the cathode, LBSM was mixed with an appropriate amount of graphite (30 wt.%) and ball-milled for 24 h to form a uniform electrode powder. Using the screen-printing method, the LBSM electrode precursor was printed to the SSZ substrates and then sintered at 900 °C for 2 h in air. The area of the printed LBSM was 1.0 cm^2. GDC was subsequently deposited into the LBSM framework with an ion-impregnating technique. 0.5 M impregnation solution of $Gd_{0.2}Ce_{0.8}(NO_3)_3$ (20 mol% $Gd(NO_3)_3$ + 80 mol% $Ce(NO_3)_3$) was prepared from Aldrich chemicals of $Gd(NO_3)_3{\cdot}6H_2O$ (99.9%) and $Ce(NO_3)_3{\cdot}6H_2O$ (99.9%). Ion-impregnation was carried out by placing a drop of the solution on top of the coating which infiltrated the cathode layer by capillary effect. The sample was then sintered at 850 °C in air for 1 h before the testing. At 850 °C the nitrate salt was decomposed, forming $Ce_{0.8}Gd_{0.2}O_{2-\delta}$ (GDC) oxide phase [21]. The mass of the electrode before and after the impregnation treatment was measured to determine the impregnated oxide loadings. The procedure was repeated to increase the GDC loadings. The impregnated GDC loadings in LBSM–GDC composite cathodes were 30, 40, 50 and 55 wt.% (named LBSM–GDC30, LBSM–GDC40, LBSM–GDC50 and LBSM–GDC55, respectively).

The polarization resistance was measured by two-electrode impedance method using symmetric cells, using AC impedance spectroscopy (ZAHNER IM6e) with a 20 mV AC signal, over a frequency range of 0.05 Hz to 1 MHz. Various phases of the powder were identified with a Rigaku X-ray diffraction (XRD) diffractometer at room temperature, using monochromatic Cu Kα radiation. The microstructure of the cathode section was studied by scanning electron microscopy (SEM). Three single cells were prepared with the LBSM cathode, the LBSM–GDC30 composite cathode and the LBSM–GDC50 composite cathode on the anode-supported SSZ film. The performance of single cells was measured from 600 to 750 °C with humidified hydrogen (a water content of around 3 vol.%) as fuel and air as oxidant. The area of each cathode was 1 cm^2. Platinum mesh, attached to the cathode surface with platinum paste, was used as the current collector. A four-probe configuration was used for electrochemical impedance spectroscopy (EIS) measurements.

3. Results and discussion

3.1. Characterization of LBSM

Fig. 1 shows the thermal expansion curves of LBSM and SSZ in air. The shape of their curves is nearly the same. Further calculation shows the average thermal expansion coefficient (TEC) of LBSM between 20 and 750 °C is $11.5 \times 10^{-6}\,K^{-1}$, and that of SSZ is $10.4 \times 10^{-6}\,K^{-1}$. The small mismatch in TEC between LBSM and SSZ is beneficial for the SOFC system in maintaining long-term stability and enduring thermal cycle. Besides, LBSM has shown a better performance than LSM [20,22], and the cathode polarization resistance (Rc) of the LBSM cathode is lower than that of the LSM cathode under the same conditions. For example, the LBSM cathode yielded Rc = 2.3, 5.3, 13.94 and 46.46 Ω cm^2 at 750, 700, 650 and 600 °C, respectively [20]. While the LSM cathode yielded Rc = 3.5, 7.82, 20.58 and 51.03 Ω cm^2 at 750, 700, 650 and 600 °C, respectively [16].

3.2. Effect of GDC loading

Fig. 2 shows the X-ray diffraction (XRD) patterns of the mixed LBSM and GDC (50 wt.%) powders after heat treatment at 850 °C for 100 h. The patterns reveal no evidence of inter-phase reactivity after heat treatment. It is concluded, therefore, that the LBSM–GDC composite cathodes are stable under the experimental conditions.

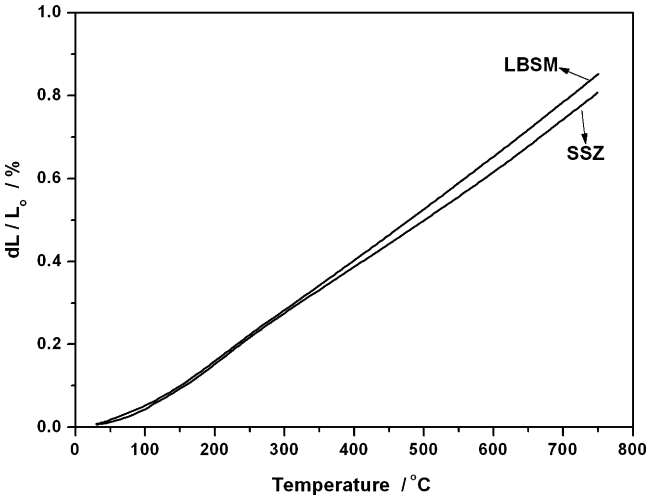

Fig. 1. Thermal expansion curves of LBSM and SSZ in air.

Fig. 3 shows the effect of the impregnated GDC loadings on the cathode polarization resistance (Rc). In general, the cathode polarization resistance of the ion-impregnated LBSM cathodes decreased as the GDC loadings increased to 50 wt.%. The value of Rc increased, however, for a further increase of the GDC loadings to 55 wt.%. This may be due to a decrease in porosity of the LBSM–GDC55 cathode, which leads to a decrease in transfer access of gas phase and an increase in concentration polarization. The low value of polarization resistances can be obtained only when the gas, ionic and electronic transportation phases present at an appropriate ratio. The optimal composition, LBSM–GDC50, yielded Rc = 0.051 and 0.097 Ω cm^2 at 750 and 700 °C, respectively. Such values are about 45 times lower than that of the cathode polarization resistance for pure LBSM. The high performance that resulted from the impregnation of GDC was due to the appropriate distribution of the GDC particles in the LBSM porous structure, which provided the effective ionic and electronic conducting pathways and, at the same time, promoted the synergistic process involving the injection of the mobile charged oxygen species into the ionic carriers.

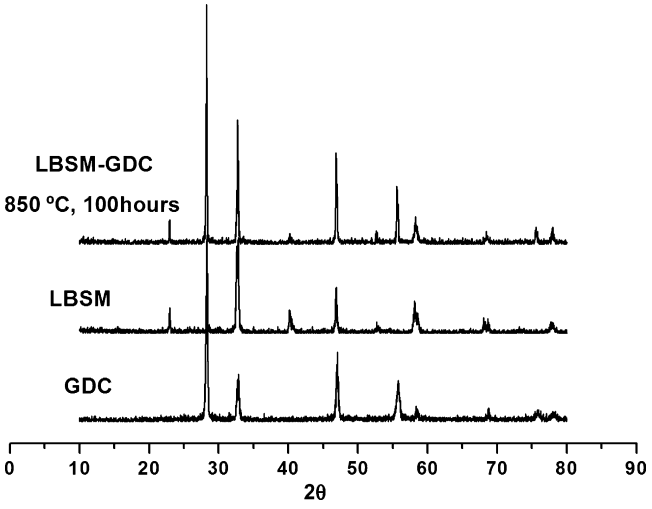

Fig. 2. XRD patterns of the mixed LBSM and GDC (50 wt.%) powders after heat treatment at 850 °C for 100 h.

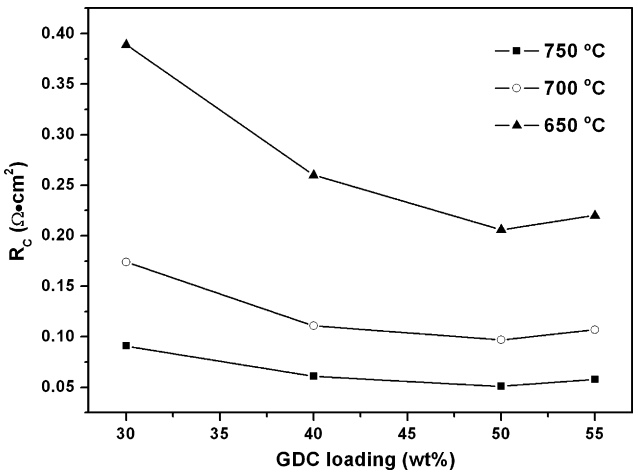

Fig. 3. Polarization resistance of the LBSM–GDC composite cathodes with various GDC loadings.

The mixed LSM-GDC50 cathode yielded Rc = 0.49 and 1.06 Ω cm^2 at 750 and 700 °C, respectively [16], and the polarization resistance of the ion-impregnated LBSM–GDC50 cathode was about 10 times lower than that of the mixed LSM-GDC50 cathode. So, the advantage of LBSM over LSM was more obvious in the composite cathodes.

Fig. 4 shows typical cross-section SEM images of the LBSM electrodes impregnated with different amounts of GDC. As shown in Fig. 4a, the screen-printed LBSM layer is highly porous, which is of great benefit for ion-impregnation. After GDC impregnation, there are very fine particles formed around the LBSM particles. The nano-sized GDC particles were deposited on the LBSM surface and in the LBSM porous structure. However, the distribution of the nano-sized GDC particles appears to be discrete and does not form a continuous network at low GDC loadings (Fig. 4b), which cannot provide sufficient ion transferring access. When the GDC loading is 50 wt.%, a continuous and porous structure of the GDC phase is most likely formed (Fig. 4c). The deposition of very fine oxygen conducting GDC particles on the LBSM surface and in the LBSM porous structure formed a mutual surrounding structure of ionic conduction phase and electronic conduction phase, which is assumed to effectively extend the triple phase boundary (TPB) for the O_2 reduction. This structure consequently leads to enhancement of the electrochemical activity and significant reduction of the cathode polarization resistance of the LBSM cathodes.

Fig. 5a shows the impedance spectra of the different cathodes measured at 750 °C in air. The values of polarization resistances were 0.091, 0.061, 0.051 and 0.058 Ω cm^2 for LBSM–GDC30, LBSM–GDC40, LBSM–GDC50 and LBSM–GDC55, respectively. Fig. 5b shows impedance spectra measured in air at 750, 700, and 650 °C for LBSM–GDC50 on the SSZ electrolyte. The equivalent circuit is also presented in Fig. 5b, modeled as the arc for LBSM–GDC50. LBSM–GDC30 and LBSM–GDC55 are also modeled well by this circuit. It is noteworthy that the impedance spectra include a major semicircle and a minor semicircle in low-frequency section. In the equivalent circuit, the inductance L is attributed to high-frequency artifacts arising from the measurement apparatus. The first resistance (R) corresponds to the resistance of the electrolyte and the lead wires. The second resistance (R_1) is the main polarization resistance for the cathode, which may be related to the resistance of oxygen surface reaction or other mechanisms. Values of R_1 at 650, 700, and 750 °C for the LBSM–GDC50 cathode were 0.193, 0.085, and 0.038 Ω cm^2, respectively. Fig. 6 shows the relationship of R_1 *versus* temperature, from which the activation energy can be calculated. The activation energy was 128, 125 and 126 kJ mol^{-1} for the ion-impregnated LBSM–GDC30, LBSM–GDC50, and LBSM–GDC55 electrodes, respectively. The activation energy for the LBSM–GDC system was almost independent of the GDC content. It was reported that the activation energies for oxide ion diffusion and the oxygen surface exchange reaction are 42 ± 2 and 113 ± 11 kJ mol^{-1}, respectively [23]. The activation energy for the LBSM–GDC system is similar to that of the oxygen surface exchange reaction, thus, we suggest that the rate-determining step of the electrode reaction may be attributed to an oxygen surface exchange reaction. The values of R_2 for the LBSM–GDC50 cathode were 0.013, 0.012 and 0.013 Ω cm^2 at 650, 700 and 750 °C, respectively, which varied little with the increased measurement temperature. R_2 is therefore very

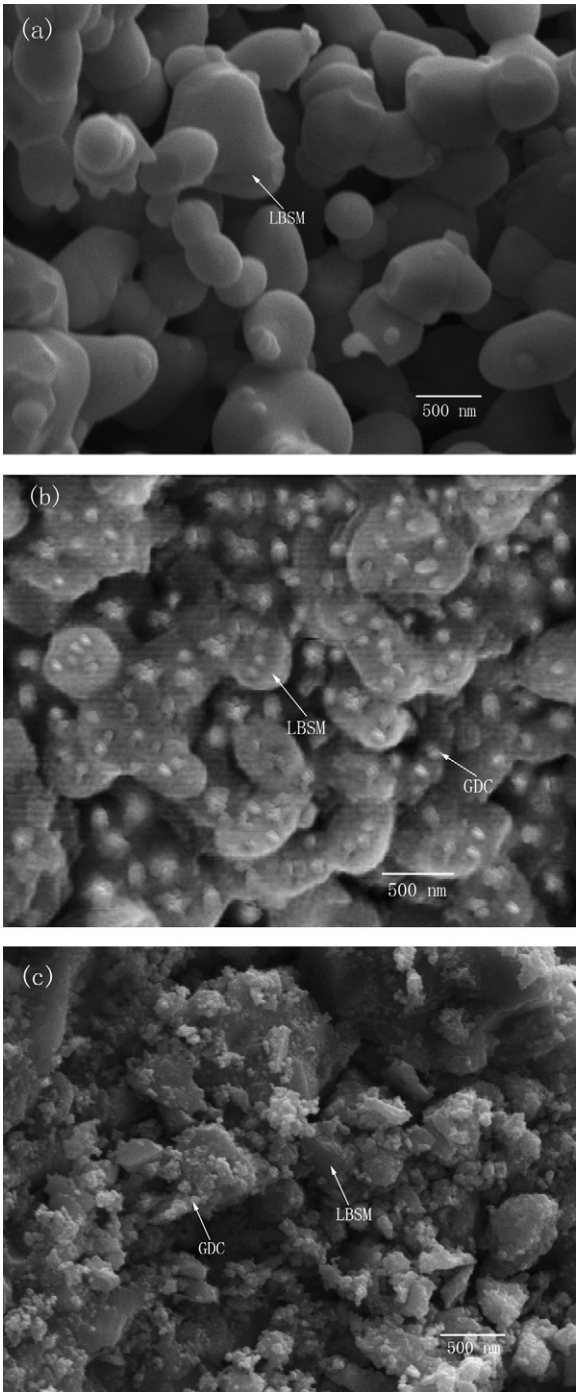

Fig. 4. Typical fracture cross-section SEM images of pure LBSM (a), LBSM–GDC30 (b) and LBSM–GDC50 (c) composite cathodes.

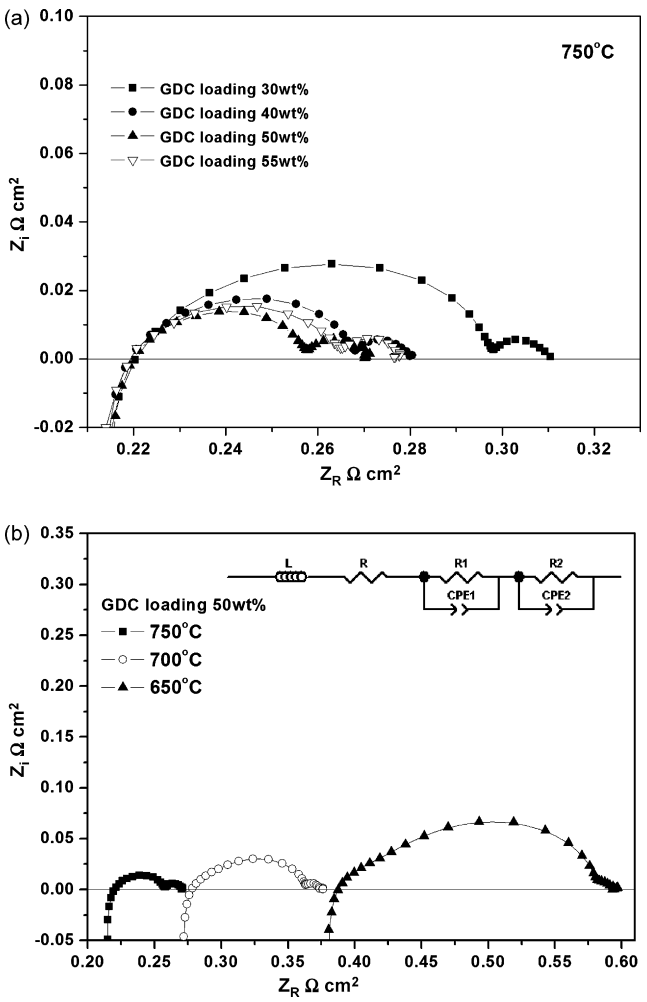

Fig. 5. AC impedance spectra of the different cathodes measured at 750 °C in air (a) and LBSM–GDC50 measured at 650, 700 and 750 °C for in air (b). The corresponding equivalent circuit is shown.

likely to be related with the diffusion of oxygen through the porous cathode [24]. The values of capacitances were about 2×10^{-3} F and 3 F for the first constant phase element (CPE1) and the second constant phase element (CPE2), respectively, and varied weakly with temperature in this composite cathode.

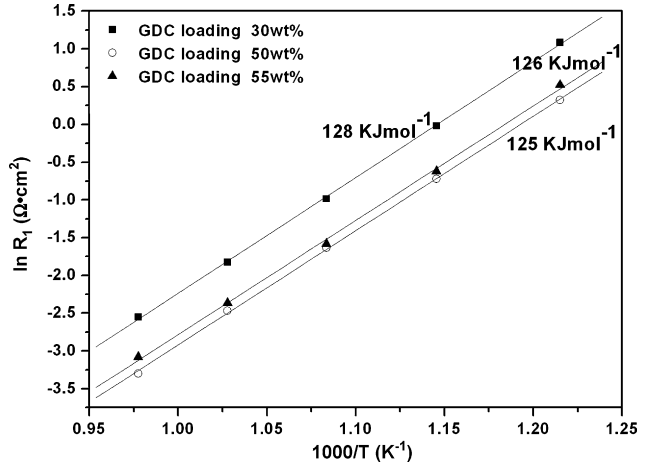

Fig. 6. Arrhenius plot of the polarization resistance for LBSM–GDC30, LBSM–GDC50 and LBSM–GDC55 cathodes.

3.3. Performance of single cells

The performance evaluation of the cells in this study was carried out by the anode-supported single cells with SSZ thin film as electrolyte. The thickness of the electrolyte and cathode was around 20 and 30 μm, respectively. Fig. 7 shows the current voltage characteristics and the corresponding power densities for three fuel cells using the LBSM cathode, the LBSM–GDC30 cathode and the

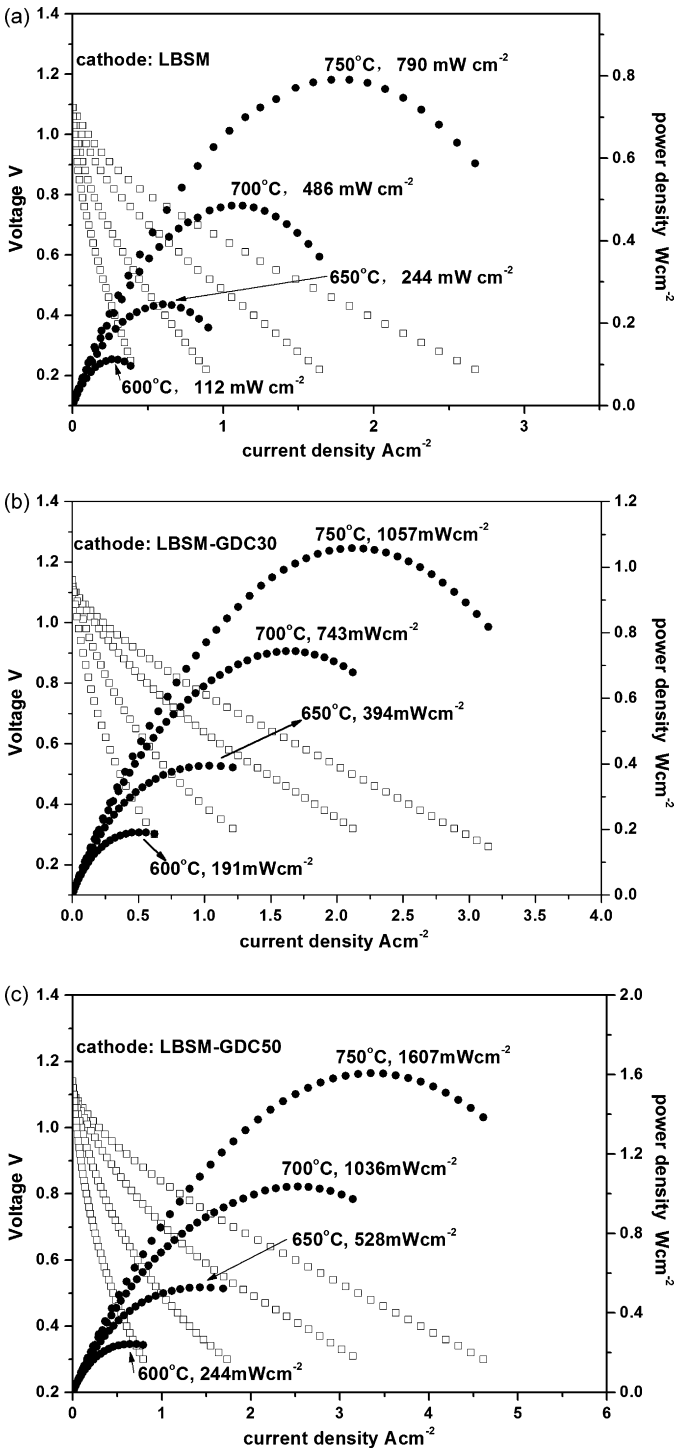

Fig. 7. The cell voltage and power density as a function of current density of the anode supported single cells with the LBSM cathode (a), the LBSM–GDC30 composite cathode (b) and the LBSM-GD50 composite cathode (c) operating at various temperatures.

LBSM–GDC50 cathode, respectively. They were measured at 600, 650, 700 and 750 °C with humidified hydrogen (a water content of around 3 vol.%) as the fuel and air as the oxidant. The maximum power densities for the cell with the LBSM cathode were 112, 244, 486, 790 mW cm^{-2} at 600, 650, 700 and 750 °C, respectively, and that of the cell with the ion-impregnated LBSM–GDC30 cathode were 191, 394, 743, 1057 mW cm^{-2} at 600, 650, 700 and 750 °C, respectively. The performance of the cell with the ion-impregnated LBSM–GDC50 cathode was higher than that of the above two cells, and the maximum power densities were 244, 528, 1036, 1607 mW cm^{-2} at 600, 650, 700 and 750 °C, respectively. For the above three cells, the anodic and electrolyte resistances could be reasonably assumed identical, because the anode and electrolyte were fabricated with the same procedures. So the relatively higher power densities resulted from the better performance of the ion-impregnated LBSM–GDC30 and LBSM–GDC50 cathodes. It demonstrates that the impregnation of the nano-sized GDC particles in the porous LBSM structure has a significant electrocatalytic effect on the activities of the LBSM cathode.

It should be noted that the formation of nano-sized GDC particles inside the porous LBSM framework, the surface areas of the impregnated ionic conducting phase would be much higher than that of pure LBSM. In addition, the high surface area and electrocatalytic materials filled the pores in the porous electrode (or at the critically important electrode/electrolyte interface), significantly boosting the three phase boundaries, which resulted in an excellent performance of the ion-impregnated LBSM–GDC system. So, the ion-impregnating method is a feasible process to develop composite cathodes. Further study should be conducted to optimize the size ratio of two different particles in the composite cathodes, and control the microstructure of the composite cathodes for improving their performance.

4. Conclusion

The LBSM–GDC composite cathodes were fabricated by ion-impregnating method, and their characteristics were investigated by AC impedance spectroscopy. The polarization resistance was significantly decreased by impregnating the electronic conducting phase (LBSM) with the ionic conducting phase (GDC). For example, the value of the cathode polarization resistance was 2.3 Ω cm^2 at 750 °C for pure LBSM cathode, but 0.091 and 0.051 Ω cm^2 for LSM-GDC30 and LBSM–GDC50, respectively. In addition, the performance of the cells was also measured and compared at various temperatures with humidified hydrogen as the fuel and air as the oxidant. The maximum power density of the cell with the LBSM cathode was 790 mW cm^{-2} at 750 °C, and that of the cell with the impregnated LBSM–GDC50 cathode was 1607 mW cm^{-2} at the same temperature. The impregnated LBSM–GDC50 cathode is shown a very promising cathode material for intermediate-temperature solid oxide fuel cells.

Acknowledgements

This work is supported financially by the Chinese High Technology Development Project (2007AA05Z151). The authors also would like to thank Prof. Changrong Xia, Chinese University of Science and Technology for his collaboration and helpful discussions.

References

[1] M. Mogenson, K.V. Jensen, M.J. Jørgensen, S. Primdahl, Solid State Ionics 150 (2002) 123–129.
[2] T. Hibino, A. Hashimoto, T. Inoue, J. Tokuno, S. Yoshida, M. Sano, Science 288 (2000) 2031–2033.
[3] K. Eguchi, J. Alloys Compd. 250 (1997) 486–491.
[4] S.P. Jiang, Solid State Ionics 146 (2002) 1–22.
[5] H.Y. Tu, Y. Takeda, N. Imanishi, O. Yamamoto, Solid State Ionics 100 (1997) 283–288.
[6] T. Kenjo, M. Nishiya, Solid State Ionics 57 (1992) 295–302.
[7] M.J.L. Østergård, C. Clausen, C. Bagger, M. Mogensen, Electrochim. Acta 40 (1995) 1971–1981.
[8] M. Juhl, S. Primdahl, C. Manon, M. Mogensen, J. Power Sources 61 (1996) 173–181.
[9] M.J. Jørgensen, S. Primdahl, M. Mogensen, Electrochem. Acta 44 (1999) 4195–4201.
[10] E.P. Murray, T. Tsai, S.A. Barnett, Solid State Ionics 110 (1998) 235–243.
[11] T. Tsai, S.A. Barnett, Solid State Ionics 93 (1997) 207–217.
[12] B.C.H. Steele, Solid State Ionics 75 (1995) 157–165.
[13] B.C.H. Steele, Solid State Ionics 86–88 (1996) 1223–1234.
[14] R. Doshi, V.L. Richards, J.D. Carter, X. Wang, M. Krumpelt, J. Electrochem. Soc. 146 (1999) 1273–1278.
[15] E.P. Murray, S.A. Barnett, Solid State Ionics 143 (2001) 265–273.
[16] S.P. Jiang, Y.J. Leng, S.H. Chan, K.A. Khor, Electrochem. Solid-State Lett. 6 (2003) A67–A70.
[17] S.P. Jiang, W. Wang, Solid State Ionics 176 (2005) 1351–1357.
[18] S.P. Yoon, J. Han, S.W. Nam, T.-H. Lim, I.H. Oh, S.-A. Hong, Y.-S. Yoo, H.C. Lim, J. Power Sources 106 (2002) 160–166.
[19] X.Y. Xu, Z.Y. Jiang, X. Fan, C.R. Xia, Solid State Ionics 177 (2006) 2113–2117.
[20] J.L. Li, S.R. Wang, Z.R. Wang, R.Z. Liu, T.L. Wen, Z.Y. Wen, J. Power Sources 179 (2008) 474–480.
[21] S.P. Jiang, Y.Y. Duan, J.G. Love, J. Electrochem Soc. 149 (2002) A1175–A1183.
[22] A. Chakraborty, H.S. Maiti, Ceram. Int. 25 (1999) 115–123.
[23] S. Lee, Y. Lim, E.A. Lee, H.J. Hwang, J.W. Moon, J. Power Sources 157 (2006) 848–854.
[24] J.D. Kim, G.D. Kim, J.W. Moon, Y.L. Park, W.H. Lee, K. Kobayashi, M. Nagai, C.E. Kim, Solid State Ionics 143 (2001) 379–389.